Zentrum für Technomathematik

Fachbereich 3 – Mathematik und Informatik

Simulation of Industrial Crystal Growth by the Vertical Bridgman Method

Stefan Boschert **Alfred Schmidt**
Kunibert G. Siebert **Eberhard Bänsch**
Klaus-Werner Benz **Gerhard Dziuk**
Thomas Kaiser

Report 00–11

Berichte aus der Technomathematik

Report 00–11 **Mai 2000**

Simulation of Industrial Crystal Growth by the Vertical Bridgman Method

Stefan Boschert[1], Alfred Schmidt[2], Kunibert G. Siebert[2], Eberhard Bänsch[3], Klaus-Werner Benz[1], Gerhard Dziuk[2], and Thomas Kaiser[1]

[1] Kristallographisches Institut, Universität Freiburg, Hebelstr. 25, D-79 104 Freiburg, Germany
http://www.krist.uni-freiburg.de
[2] Institut für Angewandte Mathematik, Universität Freiburg, Hermann-Herder-Str. 10, D-79 104 Freiburg, Germany
http://www.mathematik.uni-freiburg.de/IAM
[3] Zentrum für Technomathematik, Universität Bremen, Postfach 33 04 40, 28334 Bremen
http://www.math.uni-bremen.de/zetem

Abstract. Single crystals of Cadmium-Zinc-Telluride are used as a substrate material for the production of infrared detectors and are usually grown by the vertical Bridgman method. We present a simulation of the whole growth process in two steps: In the first step, the (stationary) heat transport in the furnace is modeled and calculated for different positions of the ampoule. This provides information about the most important parameter during this process: the temperature distribution in furnace and ampoule. The obtained temperatures are then used in the second step as boundary conditions for the (time dependent) simulation of temperature and convection in the ampoule. Only the use of adaptive finite element methods allows an efficient numerical simulation of the moving phase boundary, the convection in the melt and the temperature distribution in melt and crystal. Numerical results are presented for both furnace and ampoule simulations.

1 Introduction

Single crystals of the semiconductor Cadmium-Zinc-Telluride (Cd,Zn)Te are excellent substrate materials for growth of thin Mercury-Cadmium-Telluride (Hg,Cd)Te layers, which are used as detector material for infrared radiation, see [7]. Such (Cd,Zn)Te crystals are usually grown by the vertical Bridgman method, where an ampoule with material melt is moved in a temperature field such that the material slowly crystallizes. Fig. 1 shows the schematics of the furnace with ampoule and heating distribution.

The material, which is placed in a sealed quartz-glass ampoule, is molten in the hot area of the crystal growth furnace. To start the crystallization process, a relative motion between the furnace and the ampoule is started resulting in a temperature reduction at the lower end of the growth ampoule. When the temperature at the bottom falls below the melting temperature

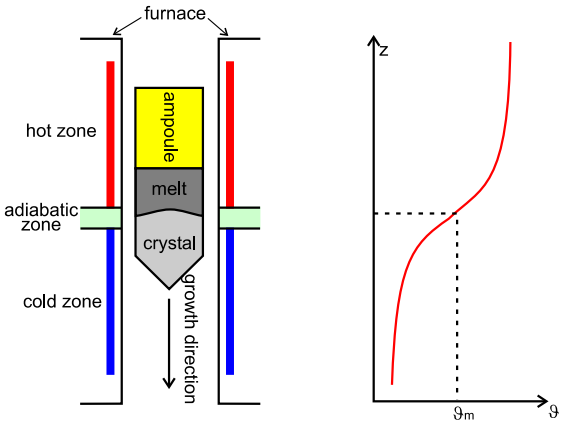

Fig. 1. Schematics of growth furnace and heating distribution.

the crystallization process starts. With further movement more and more material solidifies until finally the whole crystal is grown. The most important parameter during this process is the temperature distribution in furnace and ampoule.

In the industrial production of infrared detectors, a significant dependence of the efficiency of the manufactured detectors on the quality of the substrate material is observed. Therefore an investigation of the growth conditions for the substrate material becomes necessary, to optimize the production process. Key parameters which determine the quality of the grown crystals are the shape of the phase boundary and the temperature distribution in its vicinity. Experimental determination of such values during the growth experiment is almost impossible. To determine these temperatures, numerical simulations are a feasible way to overcome the technical problems in the direct measurement.

The simulations are performed in a two step process [5]. The first step is a global simulation of the heat distribution in the growth furnace. Here, the (stationary) heat transport in the furnace is calculated for different positions of the ampoule. To obtain the temperature distribution in the furnace, numerical simulations of the heat transport in the whole assembly have been performed similarly to [4] by a 2-D axially symmetric finite element model, using the commercial code FIDAP [11].

The second step is a local simulation of the (time dependent) phase transition and convection in the ampoule. The objective here is the investigation of the influence of convection on the moving phase boundary in the ampoule. The temperature distributions obtained from step one, the global furnace simulation, are used as boundary conditions.

The model for the local simulation consists of a Stefan problem with convection in both solid and liquid phases and the incompressible Navier-Stokes equations in the melt (compare Sec. 3). Effects of varying concentration are

neglected in the simulations presented here. Solvers for the Stefan problem and the Navier-Stokes equations on time dependent domains are combined in an adaptive finite element algorithm for the solution of the coupled system and are implemented in the adaptive finite element toolbox ALBERT [18,19]. The underlying finite element meshes are adapted to the solution in each time step using information from a posteriori error estimators. Only the use of adaptive finite element methods allows an efficient numerical simulation of the moving phase boundary, the convection in the melt, and the temperature distribution in melt and crystal.

2 Modeling of the Crystal Growth Furnace

In this section we discuss the modeling of the crystal growth furnace and the influence of the growth ampoule on the temperature distribution. Then the calculation of the heat transport and relevant results from the simulation are presented.

2.1 Furnace and Crystal Growth

The crystal growth experiments are performed in a multi-zone resistance furnace. This furnace consists of a hot zone and a cold zone, subdivided into ten sub-zones each, and separated by an adiabatic zone. The upper hot heating sub-zones are all kept at a fixed temperature (1140°C) above the melting point of (Cd,Zn)Te (1092°C). The lower cold sub-zones are adjusted to 840°C to realize a temperature gradient in the area of the adiabatic zone. For the solidification process the furnace is slowly moved upwards (30 mm/day) to generate the temperature decrease in the ampoule.

The diameter of the growth ampoule is 65 mm, and the length of the grown crystals is typically around 125 mm, resulting in crystals of about 2 kg weight. This makes it necessary to have a furnace with an inner diameter of ≈ 95 mm and a height of more than 1 m to ensure a uniform temperature distribution. Due to the fact that the temperatures in the hot area of the furnace are well above 1100°C, radiation plays an important part in the heat transport. Furthermore, convection (of the gas between furnace wall and ampoule and of the melt) as well as conduction contribute to the overall heat transport. In particular, the heat conduction in the furnace insulation is another key parameter for the heat transport in the assembly [9].

2.2 Modeling of the Heat Transport

For the calculation of the heat transport several assumptions and simplifications have to be made. Thus the convection in the furnace, either of the gas between ampoule and furnace wall and in the melt, is modeled by an effective conductivity consisting of the pure conductivity and an additional

part from convection. In the furnace insulation pure conductivity is assumed. The influence of convection (in the porous medium) is neglected as well as inhomogeneities caused by power supply, furnace control etc.

Thus the heat equation (in dimensional form) has to be solved for the temperature ϑ:

$$\rho c\, \partial_t \vartheta = \nabla(\kappa \nabla \vartheta) + H$$

where ρ is the density, c the specific heat, κ the conductivity and H gives the contribution of an volumetric heat source. On a boundary segment the general heat transfer condition for the normal heat flux q is

$$q = -\boldsymbol{n} \cdot (\kappa \nabla \vartheta) = q_c + q_r$$

which consists of a conductive part q_c and a radiative part q_r. The latter one is modeled by an additional nonlinear equation for the radiative heat exchange between all surfaces which includes mutual visibility and shadowing, see [5] for details.

In the furnace simulation the phase transition in the ampoule is not computed. But using a temperature dependent heat conductivity (different values for temperatures below or above the melting point), the distinct behavior of the solid and liquid phase is considered. The simulations are performed for several positions of the ampoule in the furnace. These values can be used as boundary conditions for the calculation of the convection/solidification problem discussed in more detail in Sec. 3. But also some valuable information for the crystal grower concerning the ampoule-design and crystal growth process can be derived, which will be presented in the following.

During industrial production, the temperature at the bottom of the crystal is monitored. Temperatures from our simulations are compared with such measurements, performed by M. Bruder (AIM, AEG Infrarot Module GmbH). A good agreement between the experimental values and the simulation is observed.

2.3 Results of the Furnace Simulation

A typical temperature distribution in the whole crystal growth assembly is shown in Fig. 2. The temperature difference between the neighbouring isotherms is 200°C. The shape of the ampoule and the melt is indicated as well. It can be seen that the ampoule is completely in the hot area of the furnace. Later, during the growth process, the ampoule is shifted downwards to start the crystallization.

An important parameter for the crystal grower is the temperature distribution in the melt and crystal at different ampoule locations in the furnace. Of special importance is the position and shape of the melting-point isotherm, which corresponds to the phase boundary in the simplified model used here.

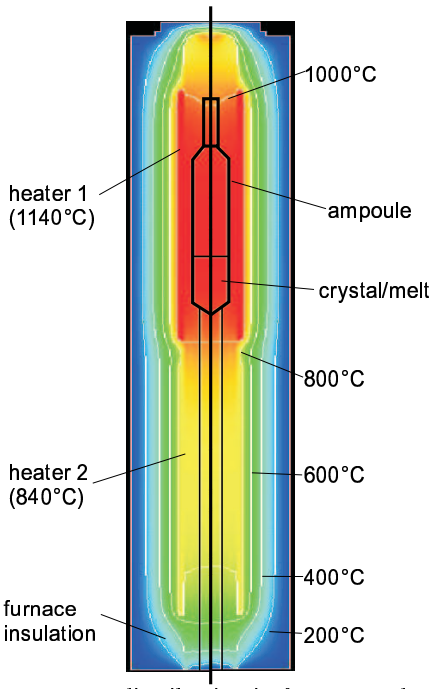

Fig. 2. Calculated temperature distribution in furnace and ampoule. The shape of the ampoule and several isotherms are given.

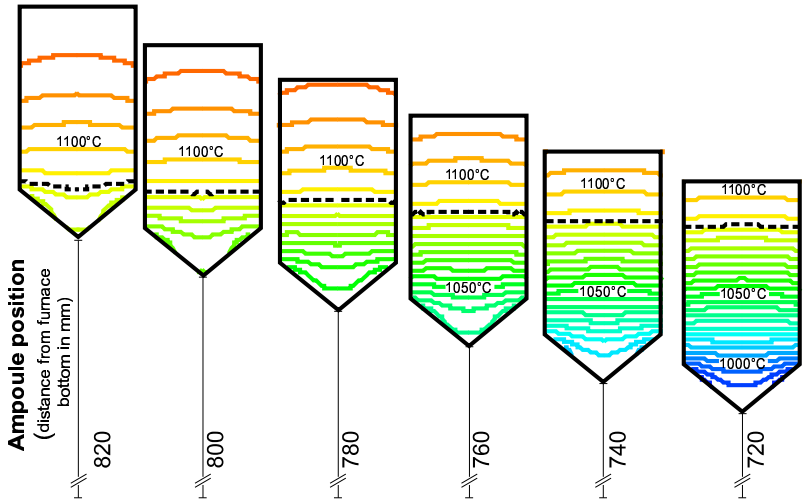

Fig. 3. Temperature distribution in crystal and melt at different ampoule positions in the furnace (ampoule position measured from bottom of furnace in mm). The temperature difference between the isotherms is 5°C. The position of the melting isotherm ($\vartheta = 1092$°C) is also marked (dashed line).

In Fig. 3 the temperature distribution for different ampoule positions is given. From left to right a larger portion of material crystallizes. The shape of the melting-point isotherm changes from slightly concave in the beginning (unfavorable for crystal growth) to slightly convex in the end. The absolute position of the phase boundary also moves downwards (during the whole experiment $\approx$ 20 mm). This means that the growth velocity is lower than the velocity of the ampoule movement. As a consequence the crystal growth process needs more time to finish than expected. Such information is important for the crystal grower because it gives proper means to plan the experiment – with the pulling rate of 30 mm/day there is nearly one day difference between the expected and the calculated end of the growth process.

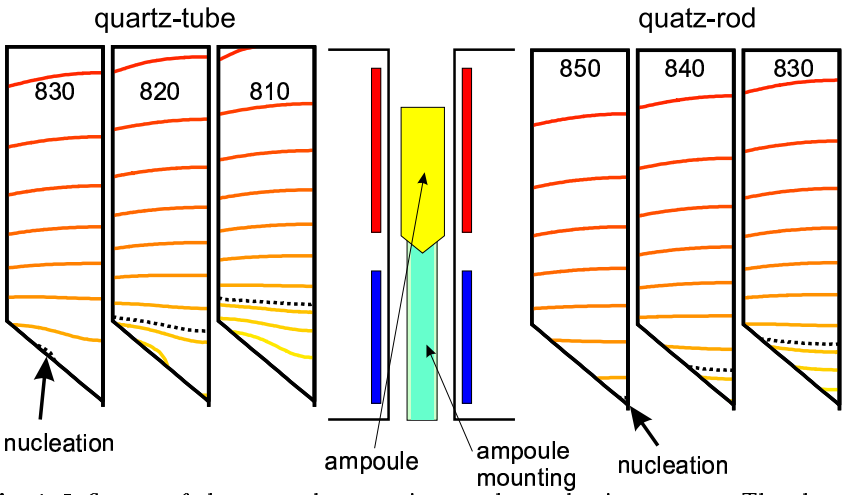

Fig. 4. Influence of the ampoule mounting on the nucleation process. The change from a quartz-glass tube (on the left) to a solid quartz rod (on the right) improves the nucleation process.

The thermal simulation can also be used to improve the design of the growth ampoule. In the original configuration the ampoule is placed upon a quartz tube during the experiment. From the simulation can be seen that this tube influences the thermal field in the beginning of the solidification process. The coldest place is not the tip of the ampoule but rather the place where ampoule and quartz tube are connected. This leads to an undesired nucleation at that place. To overcome this problem a different type of ampoule mounting has been tested: the quartz tube is replaced by a solid quartz rod. From Fig. 4 it can be seen that after this modification the position of the first nucleation is shifted to the tip of the ampoule. The undesired nucleation at the side can thus be avoided. The first crystals produced by AIM with such a modified ampoule mounting show an improved quality of the grown crystal.

3 Local Simulation in the Ampoule

In this section we investigate the influence of the convection on the moving phase boundary in the ampoule, where the results from the global furnace simulations are used as boundary conditions for the temperature at the ampoule boundary in the Stefan problem.

Once the pulling rate of the crystal growth process is given, there is a one-to-one relation between an ampoule position z in the furnace and the corresponding time t. Temperature values at the ampoule boundary are computed for a discrete number of ampoule positions by the global simulation. The piecewise linear interpolant (in time) of these discrete temperature values is used for the calculation of enthalpy boundary values u_∂ in (1c).

Using the Boussinesq approximation, the moving phase boundary and convection in the ampoule Ω are modeled by system (1)–(2) for the temperature ϑ, energy density (enthalpy) u, velocity $\boldsymbol{v}$, and pressure p. The time dependent liquid sub-domain is defined via the melting temperature ϑ_m by

$$\Omega_l(t) := \{x \in \Omega \ : \ \vartheta(x,t) > \vartheta_m\}.$$

Let k denote the heat conductivity, ρ the density, c the specific heat, L the latent heat, χ the characteristic function of the liquid phase Ω_l, η the kinematic viscosity, β_ϑ the thermal expansion coefficient, and $\boldsymbol{g}$ the vector of gravity.

The Stefan problem with convection applies in both liquid and solid phases ($\Omega = \Omega_l(t) \cup \Omega_s(t)$),

$$\begin{aligned}
\partial_t u + (\chi\,\boldsymbol{v}) \cdot \nabla u - \nabla \cdot (k \nabla \vartheta) &= 0 && \text{in } \Omega, t > 0, && \text{(1a)}\\
u &= \rho(c\vartheta + \chi L) && \text{in } \Omega, t > 0, && \text{(1b)}\\
u &= u_\partial && \text{on } \partial\Omega, t > 0, && \text{(1c)}\\
u(\cdot, 0) &= u_0 && \text{in } \Omega, && \text{(1d)}
\end{aligned}$$

and the incompressible Navier-Stokes equations hold in the liquid phase $\Omega_l(t)$,

$$\begin{aligned}
\partial_t \boldsymbol{v} - \eta \Delta \boldsymbol{v} + (\boldsymbol{v} \cdot \nabla)\boldsymbol{v} + \frac{1}{\rho}\nabla p &= (1 - \beta_\vartheta(\vartheta - \vartheta_m))\boldsymbol{g} && \text{in } \Omega_l, t > 0, && \text{(2a)}\\
\operatorname{div} \boldsymbol{v} &= 0 && \text{in } \Omega_l, t > 0, && \text{(2b)}\\
\boldsymbol{v} &= \boldsymbol{0} && \text{on } \partial\Omega_l, t > 0, && \text{(2c)}\\
\boldsymbol{v}(\cdot, 0) &= \boldsymbol{v}_0 && \text{in } \Omega_l, t = 0. && \text{(2d)}
\end{aligned}$$

The system is coupled by the convection term $(\chi\boldsymbol{v}) \cdot u$ in (1a) and the Boussinesq forcing term in (2a). The geometry for the local simulation with solid and liquid phases is shown in Fig. 5.

The solver for the ampoule problem is based on existing solvers for the classical Stefan problem and the incompressible Navier-Stokes equations, implemented using the finite element toolbox ALBERT [18,19]. The adaptive

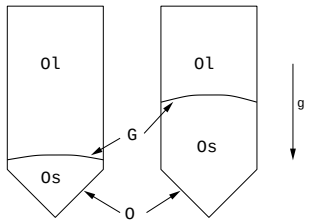

Fig. 5. Schematics of the geometry for the ampoule simulation at two different times.

method combines finite elements in space on an underlying triangulation consisting of triangles (in 2-D) and tetrahedra (in 3-D) with an appropriate discretization in time. Extensions of the standard solvers were needed to handle convection in the Stefan problem and a time dependent domain for the Navier-Stokes equations.

3.1 Adaptive Finite Element Methods for Time Dependent Problems

Given some tolerance for the error between the discrete and true solution, the aim of an adaptive method is the efficient approximation of the solution within this prescribed tolerance. For efficiency the underlying grid should be as coarse as possible but fine in regions where a high resolution is needed to keep the error below the given tolerance. Usually, these regions of high resolution move in time and thus, the underlying triangulation is adapted in each time step. Additionally, the time step size is adjusted, i. e. it is reduced if the solution changes more rapidly in time and is enlarged if the problem becomes more stationary.

Since the true solution is not known, information about the error between discrete and true solution has to be obtained by computable quantities. This goal can be achieved by *a posteriori* error estimators, which involve only information about the discrete solution and data of the problem and are thus *computable* [21]. The a posteriori error estimator is given by local indicators, contributions on single mesh elements, and by a time discretization estimator.

The adaptive method uses such estimators for the adaptation of grids and time step sizes. Meshes and time step sizes are adjusted by local refinement and coarsening of mesh elements (see Fig. 6) and reduction or enlargement of the time step size for equidistribution of local contributions over mesh elements and time steps. The aim is the reduction of computational work while the error is below the given tolerance.

Starting with an initial grid which is adapted to initial data, we construct a sequence of (variable) time step sizes and conforming triangulations. In each time step, the adaptive algorithm iteratively solves the discrete problem on the current mesh, estimates the error, and adapts the mesh and time step size until the given tolerance is reached. We start with the mesh and time

step size from the last time step. The mesh adaption is performed by local refinement and coarsening. All elements with large local indicator are marked for refinement and those elements with local indicators much smaller than the local tolerance are marked for coarsening. Coarsening is an important ingredient for time dependent problems since regions where a high resolution is needed move in time. As a consequence, the highly refined regions have to move in time, too, and parts of the previously refined regions have to be coarsened in order to keep the mesh as coarse as possible.

Additionally, the time step size is adjusted to the temporal behavior of the solution. If the time step size is reduced or the grid is refined, the discrete problem is solved again, and the adaptive process is iterated. Usually, only a small number of adaptive iterations are needed in each time step. If the changes of the solution in time are very small, an *explicit adaptive strategy* is also sufficient, where the problem is solved only once in each time step.

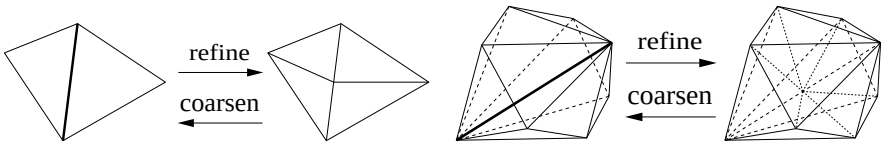

Fig. 6. Atomic refinement and coarsening operation in 2-D and 3-D.

The refinement and coarsening routines construct a sequence of nested meshes with a hierarchical structure. During mesh modifications, degrees of freedom (DOFs) are created or deleted and finite element functions must be transformed to the new finite element spaces. For example, in time dependent problems we have to transform the solution from the old time step during these modifications. Usually, these transformations can be realized by a sequence of local operations during the atomic refinement/coarsening operation, shown in Fig. 6.

ALBERT provides all tools for the local mesh modifications. It supports different finite element spaces on the same triangulation, administrates all used DOFs and all finite element data is automatically transformed during mesh modifications. For the ampoule simulation, different ansatz spaces for temperature, pressure, and velocity are used, see Sec. 3.4.

3.2 Navier-Stokes Equations on a Time Dependent Domain

For transient flow problems on fixed domains a solver for the incompressible Navier-Stokes equations is already implemented in ALBERT. The finite element discretization is based on the Taylor-Hood element using piecewise polynomials of degree p for the velocity and of degree $p-1$ for the pressure approximation. For the time discretization the so called fractional θ-scheme is used which was introduced in [6]. We use this scheme in a variant as operator

splitting, which decouples the two fundamental difficulties in the numerical treatment of the incompressible Navier-Stokes equations: the solenoidal condition and the nonlinearity. Each time step is split into three fractional steps. In the first and third step we compute a divergence free velocity field with corresponding pressure by solving a *linear saddle point problem* and handling the nonlinearity explicitly. In the second step we disregard the solenoidal condition and solve a *non-linear elliptic problem* for the velocity. This approach works well in the case of moderate Reynolds number [1,2]. The stability and convergence properties of this scheme for the time discretization of the Navier-Stokes equations are analyzed in [12,14,15].

One main difficulty for the discretization of system (2) is the fact that the domain is changing in time. The domain for the Navier-Stokes equations will shrink from the full ampoule at the beginning of the ampoule simulation to the empty set at the end. We have analyzed and implemented the following approaches for solving parabolic problems on time dependent domains.

Penalty Approach. The liquid phase is a sub-domain of the complete ampoule for all times, i.e. $\Omega_l(t) \subset \Omega$ for all $t \geq 0$. Extend given data of the differential equation to Ω and solve the equation in Ω and treat the boundary condition

$$\boldsymbol{v} = \mathbf{0} \qquad \text{on } \Gamma(t) := \partial\Omega_l(t) \setminus \partial\Omega$$

by penalizing the solution for being non zero on $\Gamma(t)$. We prove for a linear model problem [5] that this penalty approach leads to a stable discretization.

The existing solver was extended to time dependent domains by adding the penalty term. This term reduces to a boundary integral over $\Gamma(t)$ that has to be assembled into the system matrix for all parts of the fractional θ-scheme. On the one hand, the penalization part makes the resulting scheme more stable, because we add a positive semi-definite term. On the other hand, for stronger penalization this term becomes dominant and makes the system more stiff. Thus, a special preconditioning for an efficient solution of the discrete system is needed. For more details about this approach see [5].

Remark. The *fictitious domain method* was introduced in [13] for the solution of the Navier-Stokes equations on a fixed domain ω with a complicated boundary $\Gamma = \partial\omega$. The equations are solved on a bigger domain $\Omega \supset \omega$ which can be discretized more easily, and the boundary condition on Γ is treated as a constraint, similar to the solenoidal condition $\operatorname{div} \boldsymbol{v} = 0$. The objective in this approach is to avoid a complicated meshing of the domain ω but the method can directly be extended to a time dependent domain. Due to the additional constraint and the discretization of the corresponding Lagrange multiplier (jump of the normal derivatives of $\boldsymbol{v}$ across $\Gamma(t)$) this method turns out to be unstable in practice.

Sub-domain Approach. ¿From a triangulation of the whole ampoule, we construct a triangulation for the discretization of the Navier-Stokes equation by collecting all mesh elements which belong completely to the liquid phase, compare [3]. The original fractional θ-scheme is then applied on finite element spaces corresponding to this discrete sub-domain. No-slip boundary values for the velocity are prescribed explicitly on the boundary of this sub-domain. In contrast to the penalty approach, the resulting discrete linear systems do not become more stiff and can thus be solved more efficiently. Additionally, the dimensions of the finite element spaces get smaller when the liquid sub-domain shrinks.

3.3 Stefan Problem with Convection

After a Kirchhoff transformation and an appropriate scaling of variables, the equation for enthalpy u and temperature $\vartheta = \beta(u)$ reads

$$\partial_t u + \boldsymbol{v} \cdot \nabla u - \Delta\beta(u) = 0 \qquad \text{in } \Omega,\ t > 0 \tag{3a}$$

$$u = u_\partial \qquad \text{on } \partial\Omega,\ t > 0 \tag{3b}$$

$$u(\cdot, 0) = u_0 \qquad \text{in } \Omega \tag{3c}$$

Assuming piecewise constant physical coefficients in the phases, the nonlinear function β connecting temperature and enthalpy is piecewise linear, monotone, and vanishes identically for $u \in [0, 1]$, resulting in a *degenerate* parabolic equation for the energy density. The full discretization of the Stefan problem combines piecewise linear finite elements in space and a time discretization including the convection that is based on the method of characteristics [10]. Adaptive finite element methods based on a posteriori error estimates for such equations were derived in [8,16,17]. Such error indicators are used to adapt the meshes and time step sizes for the coupled ampoule problem.

3.4 Numerical Method and Results for the Ampoule Problem

We present results of two- and three-dimensional simulations for model problems. While using non physical coefficients and parameters, they show that our numerical method is able to efficiently solve the problems of phase transition and convection in the melt. Results for physical parameters as well as axisymmetric simulations are work in progress and will be published in a forthcoming paper.

The simulations are performed for an ampoule with 65 mm in diameter and 127 mm long. A fixed temperature profile, piecewise linear in z direction, is shifted vertically with a pulling rate of 0.5mm/sec to define the time dependent boundary values for the enthalpy. We use a Reynolds Number Re = 1000, corresponding to a fluid which is about twice as viscous as (Cd,Zn)Te, and a dimensionless heat conductivity $k = 1.0$ in both phases. All computations were performed with the adaptive finite element toolbox

ALBERT [18] using the the cubic/quadratic Taylor-Hood element for velocity and pressure; figures were prepared using the GRAPE visualization library [20].

We use the following semi-implicit discretization of system (2),(3). In the explicit adaptive strategy for the ampoule simulation, the sequence of calculations for time step $n+1$ is:

- Solve the Stefan problem for new temperature Θ^{n+1} and enthalpy U^{n+1} with the given velocity $\boldsymbol{V}^n$ from the last time step.
- Define the new discrete liquid phase Ω_l^{n+1}.
- Solve one time step of the fractional θ-scheme for the Navier-Stokes equations for new velocity $\boldsymbol{V}^{n+1}$ and pressure P^{n+1} with the given temperature Θ^{n+1} and liquid sub-domain Ω_l^{n+1}.
- Calculate error estimators for the Stefan problem with convection, adapt mesh and time step size.

Two-Dimensional Simulations. Figure 7 depicts interface positions and velocities at three different times from a two-dimensional simulation. While the crystal grows upward, the convection gets stronger in the beginning. This behavior continues until the crystal grows up to about 3/4 of the total ampoule height. Later, convection decreases until finally the whole domain is filled with solid material. Corresponding meshes are shown in Fig. 8. The adaptive method automatically generates highly refined meshes near the moving interface, while the meshes in the solid part are very coarse, except near the corners of the domain boundary. In order to resolve the convection, the mesh in the liquid part of the domain is refined more. The reason for the high mesh refinement at the interface can be clearly seen in Fig. 9: the enthalpy U, shown in the upper graph, varies from 0 to 1 in a very narrow region, while it distributes almost uniformly inside the solid and liquid phases. The velocity is important only in the liquid, the graph of the modulus $|\chi \boldsymbol{V}|$ is shown in the middle and the adapted mesh in the lower part of the figure. Mesh and graphs are shown for the same time as in the left part of Figs. 7 and 8.

The influence of the convection on the temperature distribution is shown in Fig. 10. It depicts the temperature gradients along the axis of symmetry of the ampoule for a simulation with and without convection. According to the Stefan condition

$$[\nabla \vartheta]_s^l = -V_\Gamma [u]_s^l,$$

the temperature gradient jumps across the interface; the size of the jump is given by the product of interface velocity V_Γ and latent heat $[u] = L$. The curve for the simulation with convection corresponds to the result shown in the middle part of Fig. 7. Especially in the important region around the solid-liquid interface (around $z = 0.058$), the gradients of the temperature are larger. On the other hand, the gradients are smaller in the upper part of

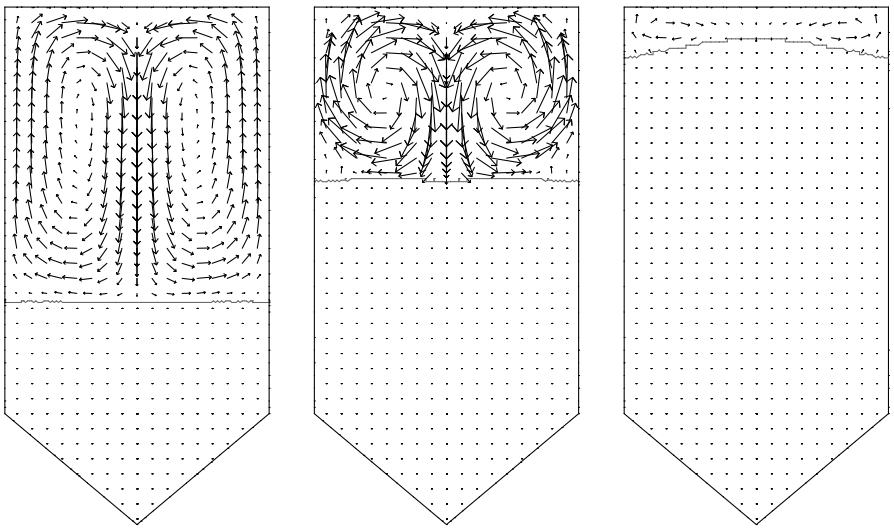

Fig. 7. 2-D simulation. Interface and convection in the melt at different times; arrow length corresponds to $|\boldsymbol{V}|$.

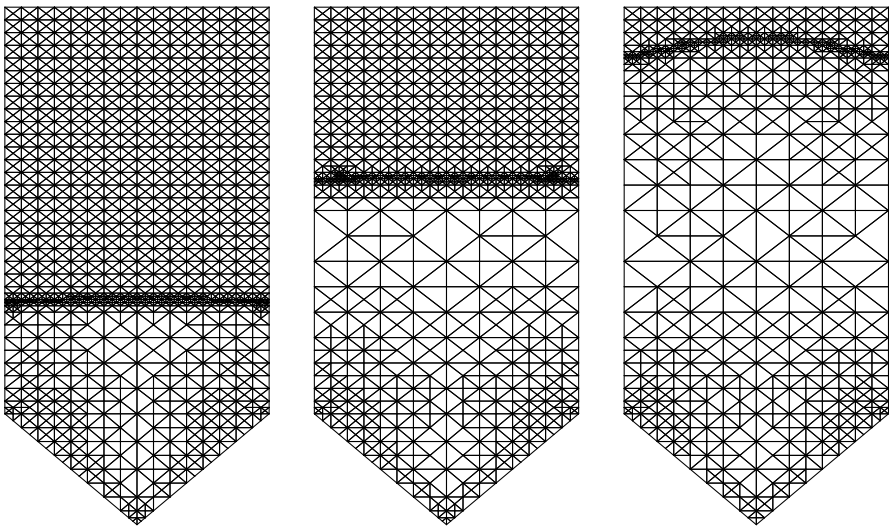

Fig. 8. 2-D simulation. Adaptive grids for same times as in Fig. 7.

the melt. The influence of the convection on the temperature gradients is not seen in the furnace simulation and underlines the necessity of the ampoule simulation. This influence is also reflected by the concave parts of the interface in the middle part of Fig. 7.

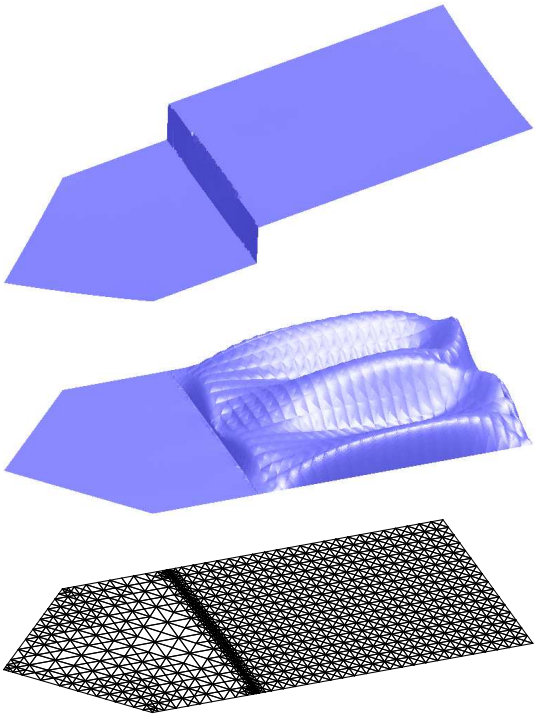

Fig. 9. 2-D simulation. Graph of enthalpy U (top), convection $|\chi \boldsymbol{V}|$ in the melt (middle) and adaptive grid (bottom).

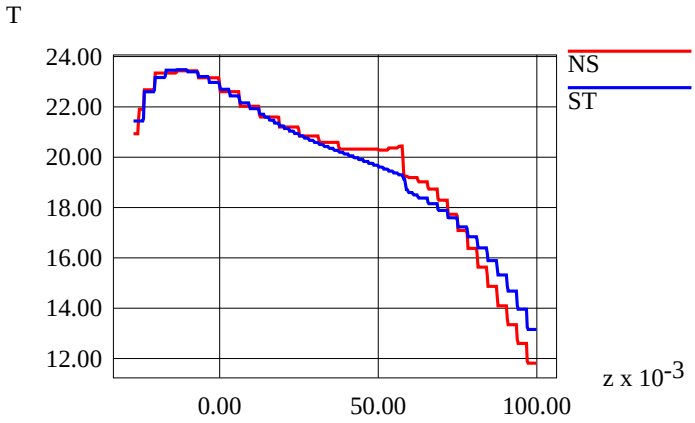

Fig. 10. 2-D simulation. Modulus of temperature gradients along the axis of symmetry for simulation with and without convection. Gradients jump across the interface which is located around $z = 0.058$.

Three-Dimensional Simulation. In three space dimensions, simulations are much more costly than in two dimensions. ALBERT allows program development in two dimensions and, with only few program modifications, simulations in three dimensions. Figure 11 presents a triangulation of the three-dimensional ampoule consisting of tetrahedra and the solid-liquid interface together with the trace of the velocity on the center plane at two different time steps from the 3-D simulation.

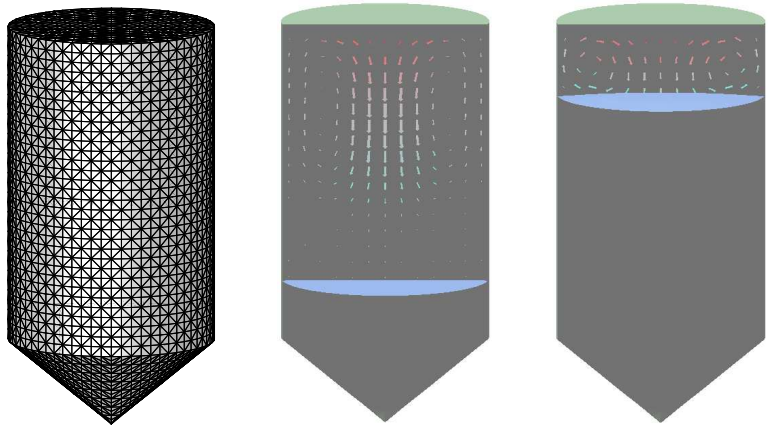

Fig. 11. 3-D simulation. Geometry and grid, interface and trace of convection on center plane at two different times.

Acknowledgement. We would like to thank Dr. M. Bruder (AIM, Heilbronn, Germany) for his collaboration and crystal growth experiments.

References

1. Bänsch, E.: An adaptive finite–element strategy for the three–dimensional time–dependent Navier–Stokes equations. J. Comput. Appl. Math. **36** (1991) 3–28
2. Bänsch, E.: Simulation of instationary, incompressible flows. Acta Math. Univ. Comenianae **LXVII** (1998) 101–114
3. Bänsch, E., Schmidt, A.: Simulation of dendritic crystal growth with thermal convection. Interfaces and Free Boundaries **2** (2000) 95–115
4. Boschert, St., Dold, P., Benz, K. W.: Modelling of the temperature distribution in a three zone resistance furnace: Influence of furnace configuration and ampoule position. J. Crystal Growth **187** (1998) 140–149
5. Boschert, St., Schmidt, A., Siebert, K. G.: Numerical simulation of crystal growth by the vertical Bridgman method. Preprint 99/24 Freiburg (1999), to appear in J.S. Szmyd and K. Suzuki (Eds.): Modelling of Transport Phenomena in Crystal Growth, Development in Heat Transfer Series, WIT Press

6. Bristeau, M. O., Glowinski, R., Periaux, J.: Numerical methods for the Navier–Stokes equations. Applications to the simulation of compressible and incompressible viscous flows. Computer Physics Reports **6** (1987) 73–187
7. Bruder, M., Schwarz, H.-J., Schmitt, R., Maier, H., Möller, M.: Vertical Bridgman growth of Cd1-yZnyTe and characterization of substrates for use in Hg1-xCdxTe liquid phase epitaxy. J. Crystal Growth **101** (1990) 266–269
8. Chen, Z., Nochetto, R. H., Schmidt, A.: A characteristic Galerkin method with adaptive error control for the continuous casting problem. Preprint 35/98 Freiburg (1998), to appear in Comp. Meth. Appl. Mech. Engrg.
9. Crochet, M., Dupret, F., Ryckmans, Y., Geyling, F., Monberg, E.: Numerical simulation of crystal growth in a vertical Bridgman furnace. J. Crystal Growth **97** (1989) 173–185
10. Douglas, Jr., J., Russell, T.: Numerical methods for convection-dominated diffusion problem based on combining the method of characteristic with finite element or finite difference procedures. SIAM J. Numer. Anal. **19** (1982) 871–885
11. Engelmann, M.: FIDAP 8.5. Fluent Inc. (1999)
12. Fernandez-Cara, E., Beltran, M.: The convergence of two numerical schemes for the Navier-Stokes Equations. Numer. Math. **55** (1989) 33–60
13. Glowinski, R., Pan, T.-W., Periaux, J.: A fictitious domain method for external incompressible viscous flow modeled by Navier–Stokes equations. Comput. Methods Appl. Mech. Engrg. **112** (1994) 133–148
14. Kloucek, P., Rys, F.: Stability of the fractional step θ–scheme for the nonstationary Navier-Stokes Equations. SIAM J. Numer. Anal. **31** (1994) 1312–1335
15. Müller-Urbaniak, S.: Eine Analyse des Zwischenschritt–θ–Verfahrens zur Lösung der instationären Navier–Stokes–Gleichungen. Preprint Heidelberg 94-01 (1994)
16. Nochetto, R. H., Schmidt, A., Verdi, C.: Adapting meshes and time-steps for phase change problems. Rend. Mat. Acc. Lincei Ser. IX **8** (1997) 273–292
17. Nochetto, R. H., Schmidt, A., Verdi, C.: A posteriori error estimation and adaptivity for degenerate parabolic problems. Math. Comp. **69** (2000) 1–24
18. Schmidt, A., Siebert, K. G.: Concepts of the finite element toolbox ALBERT. Preprint 17/98 Freiburg (1998), to appear in Notes Numer. Fluid Mech.
19. Schmidt, A., Siebert, K. G.: ALBERT: An adaptive hierarchical finite element toolbox, Documentation. Preprint 06/00 Freiburg (2000) 244 p.
20. SFB 256: GRAPE – GRAphics Programming Environment Manual, Version 5.0. Bonn (1995)
21. Verfürth, R.: A review of a posteriori error estimation and adaptive mesh-refinement techniques. Wiley & Sons, Teubner (1996)

Berichte aus der Technomathematik ISSN 1435-7968

`http://www.math.uni-bremen.de/zetem/berichte.html`

— Vertrieb durch den Autor —

Reports **Stand: 12. Mai 2000**

98–01. Peter Benner, Heike Faßbender:
An Implicitly Restarted Symplectic Lanczos Method for the Symplectic Eigenvalue Problem, Juli 1998.

98–02. Heike Faßbender:
Sliding Window Schemes for Discrete Least-Squares Approximation by Trigonometric Polynomials, Juli 1998.

98–03. Peter Benner, Maribel Castillo, Enrique S. Quintana-Ortí:
Parallel Partial Stabilizing Algorithms for Large Linear Control Systems, Juli 1998.

98–04. Peter Benner:
Computational Methods for Linear–Quadratic Optimization, August 1998.

98–05. Peter Benner, Ralph Byers, Enrique S. Quintana-Ortí, Gregorio Quintana-Ortí:
Solving Algebraic Riccati Equations on Parallel Computers Using Newton's Method with Exact Line Search, August 1998.

98–06. Lars Grüne, Fabian Wirth:
On the rate of convergence of infinite horizon discounted optimal value functions, November 1998.

98–07. Peter Benner, Volker Mehrmann, Hongguo Xu:
A Note on the Numerical Solution of Complex Hamiltonian and Skew-Hamiltonian Eigenvalue Problems, November 1998.

98–08. Eberhard Bänsch, Burkhard Höhn:
Numerical simulation of a silicon floating zone with a free capillary surface, Dezember 1998.

99–01. Heike Faßbender:
The Parameterized SR Algorithm for Symplectic (Butterfly) Matrices, Februar 1999.

99–02. Heike Faßbender:
Error Analysis of the symplectic Lanczos Method for the symplectic Eigenvalue Problem, März 1999.

99–03. Eberhard Bänsch, Alfred Schmidt:
Simulation of dendritic crystal growth with thermal convection, März 1999.

99–04. Eberhard Bänsch:
Finite element discretization of the Navier-Stokes equations with a free capillary surface, März 1999.

99–05. Peter Benner:
Mathematik in der Berufspraxis, Juli 1999.

99–06. Andrew D.B. Paice, Fabian R. Wirth:
Robustness of nonlinear systems and their domains of attraction, August 1999.

99–07. Peter Benner, Enrique S. Quintana-Ortí, Gregorio Quintana-Ortí:
Balanced Truncation Model Reduction of Large-Scale Dense Systems on Parallel Computers, September 1999.

99–08. Ronald Stöver:
Collocation methods for solving linear differential-algebraic boundary value problems, September 1999.

99–09. Huseyin Akcay:
Modelling with Orthonormal Basis Functions, September 1999.

99–10. Heike Faßbender, D. Steven Mackey, Niloufer Mackey:
Hamilton and Jacobi come full circle: Jacobi algorithms for structured Hamiltonian eigenproblems, Oktober 1999.

99–11. Peter Benner, Vincente Hernández, Antonio Pastor:
On the Kleinman Iteration for Nonstabilizable System, Oktober 1999.

99–12. Peter Benner, Heike Faßbender:
A Hybrid Method for the Numerical Solution of Discrete-Time Algebraic Riccati Equations, November 1999.

99–13. Peter Benner, Enrique S. Quintana-Ortí, Gregorio Quintana-Ortí:
Numerical Solution of Schur Stable Linear Matrix Equations on Multicomputers, November 1999.

99–14. Eberhard Bänsch, Karol Mikula:
Adaptivity in 3D Image Processing, Dezember 1999.

00–01. Peter Benner, Volker Mehrmann, Hongguo Xu:
Perturbation Analysis for the Eigenvalue Problem of a Formal Product of Matrices, Januar 2000.

00–02. Ziping Huang:
Finite Element Method for Mixed Problems with Penalty, Januar 2000.

00–03. Gianfrancesco Martinico:
Recursive mesh refinement in 3D, Februar 2000.

00–04. Eberhard Bänsch, Christoph Egbers, Oliver Meincke, Nicoleta Scurtu:
Taylor-Couette System with Asymmetric Boundary Conditions, Februar 2000.

00–05. Peter Benner:
Symplectic Balancing of Hamiltonian Matrices, Februar 2000.

00–06. Fabio Camilli, Lars Grüne, Fabian Wirth:
A regularization of Zubov's equation for robust domains of attraction, März 2000.

00–07. Michael Wolff, Eberhard Bänsch, Michael Böhm, Dominic Davis:
Modellierung der Abkühlung von Stahlbrammen, März 2000.

00–08. Stephan Dahlke, Peter Maaß, Gerd Teschke:
Interpolating Scaling Functions with Duals, April 2000.

00–09. Jochen Behrens, Fabian Wirth:
A globalization procedure for locally stabilizing controllers, Mai 2000.

00–10. Peter Maaß, Gerd Teschke, Werner Willmann, Günter Wollmann:
Detection and Classification of Material Attributes – A Practical Application of Wavelet Analysis, Mai 2000.

00–11. Stefan Boschert, Alfred Schmidt, Kunibert G. Siebert, Eberhard Bänsch, Klaus-Werner Benz, Gerhard Dziuk, Thomas Kaiser:
Simulation of Industrial Crystal Growth by the Vertical Bridgman Method, Mai 2000.